

Magnetism in strained graphene dots

J. Viana-Gomes¹, Vitor M. Pereira², and N. M. R. Peres¹

¹ *Department of Physics and Center of Physics, University of Minho, P-4710-057, Braga, Portugal and*

² *Department of Physics, Boston University, 590 Commonwealth Avenue, Boston, Massachusetts 02215, USA*

(Dated: October 22, 2009)

We study the magnetization of square and hexagonal graphene dots. It is shown that two classes of hexagonal dots have a second order phase transition at a critical Hubbard energy U , whose value is similar to the one in bulk graphene, albeit the dots do not have a density of states proportional to the absolute value of the energy, relatively to the Dirac point. Furthermore, we show that a particular class of hexagonal dots having zig-zag edges, does not exhibit zero energy edge states. We also study the effect of uniaxial strain on the evolution of the magnetization of square dots, and find that the overall effect is an enhancement of magnetization with strain. The enhancement can be as large as 100% for strain of the order of 20%. Additionally, stress induces a spatial displacement of the magnetization over the dot, moving it from the zig-zag to the armchair edges.

PACS numbers: 73.20.-r, 73.20.At, 73.21.Ac, 73.22.-f, 73.22.Gk, 81.05.Uw

I. INTRODUCTION

Nowadays, the terms *wonder material* and *graphene dreams*^{1,2} frequently accompany the description of the unusual electronic^{3,4,5}, thermal⁶, and mechanical properties of graphene^{8,9,10}. One of the most promising *graphene dreams* is its application to a new generation of nanoelectronic devices¹¹. To that effect, a number of systems have already been experimentally investigated, namely: single-electron transistors¹², quantum interference devices¹³, and graphene dots^{14,15}. The presence of Coulomb oscillations in graphene quantum dots was also identified by different groups^{12,14,15}.

Theoretically, the first investigations in this context focused on the transport properties of short (and wide) ribbons¹⁶. For long graphene ribbons¹⁷, it was shown that the low bias current flowing through the bulk of the ribbon is very robust with respect to a variety of constriction geometries and edge defects, a result also confirmed for disordered armchair nanoribbons¹⁸. As in the case of short ribbons¹⁶, evanescent waves were seen to play an important role in the electronic transport through graphene quantum dots¹⁹. The role of magnetic fields in the electronic levels of graphene quantum dots has been investigated by several authors. Of particular interest for transport properties is the fact that optical properties can be tuned by the size and edge type of the dot²⁰. The shape and symmetry^{21,22} of the dots also play an important role on energy level statistics and charge density. For the special case of triangular quantum dots²², the existence of “ghost states” was revealed, when these dots have armchair edges, whereas for triangular dots with zigzag edges the well known surface states are present. Of particular importance was the demonstration of large insensitivity of the electronic structure to the edge roughness²².

The main motivation for research in graphene quantum dots and ribbons is related to the need of producing a graphene-based system with an energy gap, which is not present in bulk graphene. This fact is a recognized shortcoming of bulk graphene, in what concerns applications relying on current electronic operation. Gaps can be induced by electronic quantum confinement in narrow armchair ribbons²³, a result confirmed by *ab-initio* calculations²⁵, and experimentally²⁴.

First principle calculations further show that zig-zag ribbons can support magnetic ground states which leads to a gapped spectrum²⁵. Spin polarized ground states are also present in small graphene derivative molecular systems²⁶. This finding opens a new line of research: the study of spin polarized ground states of graphene quantum dots of different geometries. In both single^{25,26} and bilayer²⁷ zig-zag ribbons, it was found that opposite edges align antiferromagnetically, with the magnetization rapidly decaying towards the bulk of the ribbon. Hartree-Fock (HF) calculations are specially suited for this type of study, since one can study the effect of different values of the Coulomb interaction on the magnetic structure. An interesting effect emerges from such studies²⁷: graphene ribbons have no critical Hubbard interaction, U , and thus the HF ground state is always magnetic. This result is at odds with the behavior of bulk graphene^{28,29,30,31} and bilayer graphene^{27,32,33}. This richness of different behaviors suggests studying the formation of magnetic ground states in graphene dots, a line a research we carry on in this paper from an HF point of view.

Interest in magnetism of sp^2 carbon systems was greatly spurred by experiments with proton-irradiated graphite³⁴, and with the experimental evidence that the measured magnetism might stem from π -orbital physics alone³⁵. Proton irradiation induces spatially disordered vacancies in the system^{44,45}. The magnetism found experimentally is supported theoretically by Hartree-Fock and *ab-initio* studies⁴³. Recent experimental developments addressed the intrinsic ferromagnetism in HOPG graphite, originating from the naturally occurring grain boundaries, where zig-zag edges develop and local magnetic moments are formed. Typical hysteretical curves of a ferromagnetic material are seen in a temperature range from 5 K up to 300 K³⁶.

Hence, disorder, such as those line defects studied recently, is a possible route for ferromagnetism in carbon-based materials. However, disorder is not a necessary condition for magnetism in sp^2 systems. It is by now well established theoretically that graphene systems with zig-zag edges can support magnetic moments and, in a system with perfect edges, this leads to magnetic ground states. An argument widely used against this result is based on the fact that the atoms at the

edges are, essentially, gigantic free radicals, which would be impossible to realize in a true graphene system. This argument ignores, however, the fact that such *gigantic free radicals* can be chemically passivated with other chemical species, notably hydrogen. It is found *ab-initio* that the long range magnetic order is robust, even under passivation of the edges²⁵, confirming early predictions³⁸.

In small graphene structures (triangles and hexagons), magnetism has been thoroughly investigated³⁹ both using *ab-initio* and Hartree-Fock methods, but generally for small dot sizes. The interplay between transport and magnetism has also been addressed⁴⁰, as well as magnetism induced by vacancies⁴¹ (which can be seen as a three site zig-zag edge).

Another topic of experimental research that has recently seen a considerable upsurge, is the study of interplay between the mechanical properties of graphene and its electronic structure. The motivation for these studies is the possibility of tailoring the transport properties of graphene by means of externally induced strain⁴⁶. Naturally related is the question of how can the above mentioned magnetic properties of graphene ribbons and dots be modified by external stress. In a previous work⁴⁷, some of the present authors showed that the electronic spectrum of graphene can be strongly modified by external stress. In particular, stress along the zig-zag edges of the system might eventually lead to the opening of a gap at large deformations. In addition to studying the magnetic properties of quantum dots in equilibrium, here we will also address how their magnetization is affected by external stress.

Our main findings can be summarized as follows. The existence of magnetic ground states in graphene dots of nano to mesoscopic sizes depends on their geometry, and not only on the existence of zig-zag portions along their edges. Within a Hartree-Fock framework, the existence (or not) of a minimum on-site Coulomb repulsion, U_c , for the onset of magnetism depends critically on the dot geometry and symmetry. When strain is applied, the nearest-neighbor hopping integrals are naturally modified. This leads to a modification of the local magnetic moments found in the ground state, in a way which is much stronger than one would expect just by calculating the isotropic renormalization of the critical Coulomb repulsion U . Our results show that magnetism is enhanced under uniaxial strain, and causes a reduction of U_c , for the dots which exhibit finite U_c . Moreover, we find that, under strain, the local magnetic moments associated with zig-zag edges in rectangular dots can drift from the zig-zag to the armchair edges.

The paper is organized as follows: in Sec. II we introduce our theoretical model, and discuss the relevance of several Coulomb terms in defining an effective Coulomb interaction U . A discussion of the appropriate value of U for graphene ensues. In Sec. III we study the magnetization of different types of square and hexagonal graphene dots. In Sec. IV the role of strain on the magnetization of graphene dots is considered. Our main results are discussed in Sec. V.

II. MODEL

Our study of magnetism in graphene quantum dots and antidots relies on the Hubbard model with on-site interaction, an approach used by other authors in the study of graphene ribbons⁴³. Since dots have no translation symmetry, the problem is solved in real space. To that end, we need to set up the Hamiltonian in a matrix form, which requires a convenient algorithm to build such a matrix for the different type of dots. In what follows we describe the model, together with the physically relevant values of the on-site Coulomb interaction.

The study of magnetism in condensed matter physics is traditionally, and frequently, based upon the Hubbard model, which can be written as

$$H = H_0 + H_U, \quad (1)$$

$$H_0 = -t \sum_{\mathbf{r}, \delta, \sigma=\uparrow, \downarrow} a_{\sigma}^{\dagger}(\mathbf{r}) b_{\sigma}(\mathbf{r} + \delta) + \text{H.c.}, \quad (2)$$

$$H_U = U \sum_{\mathbf{r}} a_{\uparrow}^{\dagger}(\mathbf{r}) a_{\uparrow}(\mathbf{r}) a_{\downarrow}^{\dagger}(\mathbf{r}) a_{\downarrow}(\mathbf{r}), \\ + U \sum_{\mathbf{r}} b_{\uparrow}^{\dagger}(\mathbf{r}) b_{\uparrow}(\mathbf{r}) b_{\downarrow}^{\dagger}(\mathbf{r}) b_{\downarrow}(\mathbf{r}). \quad (3)$$

For graphene the hopping integral is $t \simeq 2.7$ eV (used as the energy unit in this work), U is the on-site Coulomb repulsion energy, and $a_{\sigma}^{\dagger}(\mathbf{r})$ [$b_{\sigma}^{\dagger}(\mathbf{r})$] is the electronic creation operator at site A [site B] of the unit cell \mathbf{r} in the honeycomb lattice (see Fig. 1).

The Coulomb term is treated at the mean-field level^{27,30} by making the replacement of the quartic interaction by

$$H_U \rightarrow H_U^{MF} = U \sum_{\mathbf{r}, \sigma} a_{\sigma}^{\dagger}(\mathbf{r}) a_{\sigma}(\mathbf{r}) \langle a_{-\sigma}^{\dagger}(\mathbf{r}) a_{-\sigma}(\mathbf{r}) \rangle, \\ + U \sum_{\mathbf{r}, \sigma} b_{\sigma}^{\dagger}(\mathbf{r}) b_{\sigma}(\mathbf{r}) \langle b_{-\sigma}^{\dagger}(\mathbf{r}) b_{-\sigma}(\mathbf{r}) \rangle, \quad (4)$$

such that, when $\sigma = \uparrow, \downarrow$, we have $-\sigma = \downarrow, \uparrow$. After this transformation, the quantum problem becomes bi-linear in the electronic operators, and can be solved by diagonalization of two matrices of dimension $D \times D$, where D is the total number of lattice sites in the dot. The electronic density has to be determined self-consistently and the mean-field equations read⁴⁸

$$n_{a, \sigma}(\mathbf{r}) = \langle a_{\sigma}^{\dagger}(\mathbf{r}) a_{\sigma}(\mathbf{r}) \rangle, \quad (5)$$

$$n_{b, \sigma}(\mathbf{r}) = \langle b_{\sigma}^{\dagger}(\mathbf{r}) b_{\sigma}(\mathbf{r}) \rangle. \quad (6)$$

Here $n_{a, \sigma}(\mathbf{r})$ and $n_{b, \sigma}(\mathbf{r})$ are the mean electronic densities of spin σ at the A and B sites of the unit cell \mathbf{r} , respectively. The wave function of the system corresponding to an energy $E_{\lambda, \sigma}$ is labeled by the quantum number λ , having the explicit form

$$|\psi_{\lambda, \sigma}\rangle = \sum_{\mathbf{r}} A_{\lambda, \sigma}(\mathbf{r}) |a, \mathbf{r}\rangle + B_{\lambda, \sigma}(\mathbf{r}) |b, \mathbf{r}\rangle, \quad (7)$$

where $|a, \mathbf{r}\rangle$ and $|b, \mathbf{r}\rangle$ are lattice-position basis-states. The mean field equations (5) and (6) are determined as function

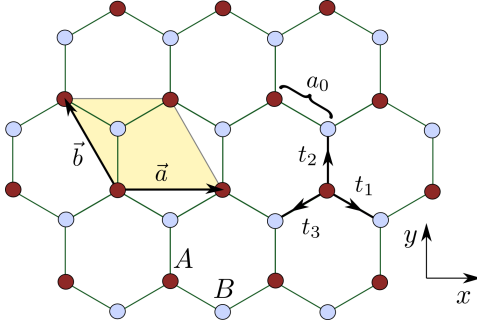


FIG. 1: (Color online) Illustration of the honeycomb lattice with the A and B sublattices, the lattice vectors δ_i ($i = 1, 2, 3$), the primitive vectors \mathbf{a} and \mathbf{b} , and the hoppings t_i ($i = 1, 2, 3$) used in Sec. IV. The abscissas are along the zig-zag edge (horizontally in the figure), and a_0 is the equilibrium carbon-carbon distance.

of the $A_{\lambda,\sigma}(\mathbf{r})$ and $B_{\lambda,\sigma}(\mathbf{r})$ coefficients, defined in the wave function (7), according to

$$n_{a,\sigma}(\mathbf{r}) = \sum_{\lambda} |A_{\lambda,\sigma}(\mathbf{r})|^2 f(E_{\lambda,\sigma}), \quad (8)$$

$$n_{b,\sigma}(\mathbf{r}) = \sum_{\lambda} |B_{\lambda,\sigma}(\mathbf{r})|^2 f(E_{\lambda,\sigma}), \quad (9)$$

where $f(x) = (1 + e^{\beta(x-\mu)})^{-1}$, μ is the chemical potential and $\beta = 1/(k_B T)$, with T the temperature. The problem has to be solved numerically. We start with a trial solution for $n_{a,\sigma}(\mathbf{r})$ and $n_{b,\sigma}(\mathbf{r})$; then the Hamiltonian is diagonalized and new values for $n_{a,\sigma}(\mathbf{r})$ and $n_{b,\sigma}(\mathbf{r})$ are computed; the procedure is iterated a number of times until convergence is reached.

As mentioned, the conventional treatment of magnetism in graphite and graphene at the Hartree-Fock level includes only the effect of the on-site Coulomb interaction U . We now discuss the importance of more general interactions⁵². We first note that, at the mean-field level, a nearest neighbor Coulomb interaction does not contribute to the existence of a ferromagnetic phase in the case of a system with translational invariance and a single orbital per unit cell⁵³. If in graphene we consider a Coulomb term of the form

$$H_V = V \sum_{\mathbf{r}, \delta, \sigma, \sigma'} a_{\sigma}^{\dagger}(\mathbf{r}) a_{\sigma}(\mathbf{r}) b_{\sigma'}^{\dagger}(\mathbf{r} + \delta) b_{\sigma'}(\mathbf{r} + \delta), \quad (10)$$

it remains true that such interaction will not contribute (at the Hartree-Fock level) to the existence of a magnetic ground state in the thermodynamic limit. The situation is different, though, in a system without translational invariance, since the spin density in neighboring carbon atoms is not necessarily equal. This is of special relevance near the edges of the system.

The mean field Hamiltonian has the form

$$H_V \rightarrow H_V^{MF} = V \sum_{\mathbf{r}, \sigma} a_{\sigma}^{\dagger}(\mathbf{r}) a_{\sigma}(\mathbf{r}) \bar{n}_b(\mathbf{r}) + (a \leftrightarrow b), \quad (11)$$

where $(a \leftrightarrow b)$ in Eq. (11) is a shorthand notation for a term with the same form as the first, but with the role of the a and

b operators interchanged, and

$$\bar{n}_b(\mathbf{r}) = \sum_{\delta, \sigma'} \langle b_{\sigma'}^{\dagger}(\mathbf{r} + \delta) b_{\sigma'}(\mathbf{r} + \delta) \rangle, \quad (12)$$

is the average density at the B neighbor carbon atoms of a given A atom at position \mathbf{r} . The terms H_U and H_V are direct Coulomb interactions. An exchange term can also be included in the Hamiltonian, having the form

$$H_J = \frac{J}{2} \sum_{\mathbf{r}, \delta} \mathbf{S}_a(\mathbf{r}) \cdot \mathbf{S}_b(\mathbf{r} + \delta), \quad (13)$$

with $S_a(\mathbf{r})$ [$S_b(\mathbf{r})$] the electronic spin operator of an electron at site \mathbf{r} of the sub-lattice A [B]. In this case, the mean field Hamiltonian is

$$H_J \rightarrow H_J^{MF} = \frac{J}{2} \sum_{\mathbf{r}, \sigma} a_{\sigma}^{\dagger}(\mathbf{r}) a_{\sigma}(\mathbf{r}) \bar{\Sigma}_b(\mathbf{r}) + (a \leftrightarrow b), \quad (14)$$

with

$$\bar{\Sigma}_b(\mathbf{r}) = \sum_{\delta, \sigma'} \sigma' \langle b_{\sigma'}^{\dagger}(\mathbf{r} + \delta) b_{\sigma'}(\mathbf{r} + \delta) \rangle, \quad (15)$$

where $\Sigma_b(\mathbf{r})$ is the average spin density at the B neighbor of a given A atom at position \mathbf{r} , and σ takes the values ± 1 when used as a multiplicative factor.

We shall assume that the leading overall effect of these three interactions can be captured by a renormalized Hubbard interaction, U , in the mean field calculations. Thus the value of U should reflect this effective interaction, rather than the bare on-site Coulomb repulsion in graphene.

We now proceed to study the ground state of dots and their magnetization as a function of U . A natural question immediately arises: what value of effective U should one take to be consistent with the magnitude of the real Coulomb interactions in the material. For the benzene molecule U was seen to be as large as 16 eV⁴⁹. In a recent study of magnetism in disordered graphene and irradiated graphite⁴³, the value of U was considered to be in the interval 3-3.5 eV, based on the value accepted for *trans*-polyacetylene, a one-dimensional bipartite sp^2 carbon system (although this value of U for *trans*-polyacetylene has been subject to controversy⁵⁰). Other two recent studies^{39,51} took $U = 2$ eV and $U = 3.85$ eV, values that reproduce the LDA gap in graphene ribbons²⁵ and the HOMO-LUMO gap in small graphene based structures. We shall consider below $U = 2$ eV and $U = 3.5$ eV as reference values in our calculations.

III. $\Delta(N)$ AND MAGNETIZATION

The results for the magnetization of graphene dots depend on the type of edges present. Generally speaking, one expects to see larger magnetization close to zig-zag edges, where the existence of localized states satisfies a spatial Stoner criterion for finite values of U ⁵⁴. The existence of such type of states is shown to be related to lattices with an odd number of

sites⁵⁵. For models with sub-lattice symmetry, as is the case of graphene, the number of zero energy modes is determined from the difference $|N_A - N_B|$, where N_A and N_B is the number of sites in sub-lattice A and B respectively^{55,56}.

In our calculations we use relatively small dots. This choice is justified because there are almost no visible finite-size effects, as we explicitly show below by studying dots of different sizes. Additionally, our choice is also justified from an experimental point of view, since it recently became possible to cleave graphene crystalites down to one-dimensional chains by irradiation inside a transmission electron microscope [see Fig. 2 of Ref. 57]. With such new experimental methods, tailoring dots of any possible size and shape seems now quite within reach.

It is useful for latter use to introduce the quantity $\Delta(N)$, as the energy interval between the highest hole state and the first particle one, for the system without interactions ($U = 0$):

$$\Delta(N) = E_{\text{lowest}}^{\text{particle}} - E_{\text{highest}}^{\text{hole}}, \quad (16)$$

where N is the total number of atoms in the dot. We consider two types of dots, with square and hexagonal shapes, and also the case of a dot with two non-connected regions (some times referred to as an anti-dot).

We start with the study of hexagonal dots. There are hexagonal dots with different symmetries and different types of edges:

1. dots with D_6 symmetry, having only armchair edges (see Fig. 2 a)).
2. dots with D_6 symmetry, having armchair and zig-zag edges (see Fig. 2 b)).
3. dots with D_3 symmetry, having armchair and zig-zag edges (see Fig.2 c)).

The first type of dot defined above shows that it is possible to have dots without zig-zag edges, no matter how large they are, and therefore the physics associated with zig-zag edges should not be present. This type of D_6 dot, when very large, is almost equivalent to the bulk system, having the full symmetry of the honeycomb lattice and therefore showing a second order phase transition at a (mean-field) critical Hubbard interaction, U_c , given by

$$U_c \simeq 2.23t, \quad (17)$$

as shown in Fig. 4 (HEX2-type). The same holds true for the D_6 HEX1-type of hexagons, but with a smaller value of U_c (smaller than 2). The dependence of the maximum value of magnetization as a function of U for the two D_6 hexagons is plotted in Fig. 4. There we see that the critical U is close to that given by Eq. (17), without any noticeable variation with the size, L , of the hexagon. In Fig. 4 the reference values for U discussed at the end of Sec. II are represented as vertical dashed lines. Clearly, the magnetic transition is well above those reference values for U , meaning that this type of dots, if experimentally fabricated, should exhibit no magnetic order.

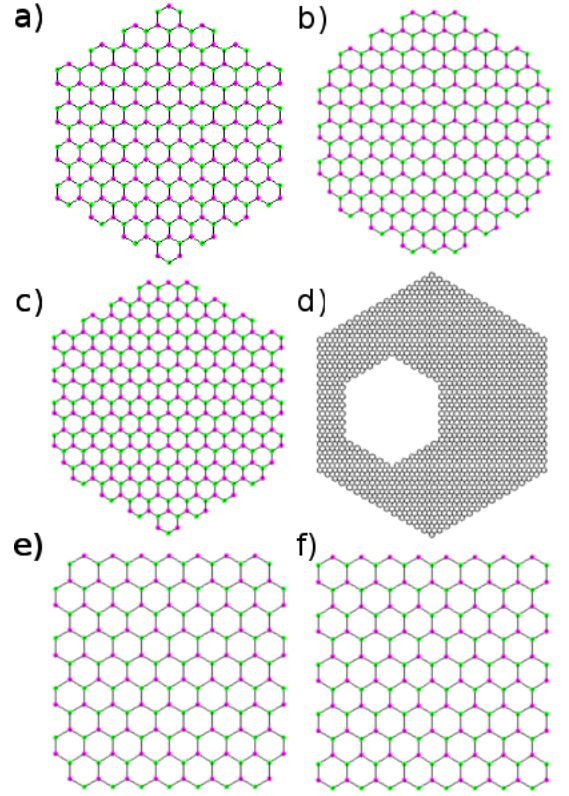


FIG. 2: (Color online) Types of hexagonal and square dots studied in this work: (a) hexagon with D_6 symmetry and no zig-zag edges (termed HEX2 in the figures below); (b) hexagon with D_6 symmetry and zig-zag edges (termed HEX1 in the figures below); (c) hexagon with D_3 symmetry with zig-zag edges; (d) an anti-dot with the external and internal boundaries made of D_6 symmetry with no zig-zag edges; (e) square where the vertices are of zig-zag type (termed SQR1); (f) square where the vertices are of armchair type (termed SQR2). The size of the figures is characterized by the number L of carbon atom horizontal-lines (zig-zag type of lines); for example, in panel (a) one has $L = 14$, and in panels (e) and (f) one has in both cases $L = 10$.

We note that the two D_6 hexagons have finite $\Delta(N)$ values, which vary as a power law with N , as shown in Fig. 5. For the HEX1- and EXH2-types of hexagons we numerically extract:

$$\Delta(N) \simeq 1.71N^{-0.53}, \quad (18)$$

$$\Delta(N) \simeq 1.75N^{-0.48}, \quad (19)$$

respectively. The exponent in the above power laws is essentially equal to $\frac{1}{2}$, and, therefore, reflects the finite-size quantization of the electronic spectrum. For square dots, on the other hand, we find that $\Delta(N)$ vanishes much rapidly as N increases, reflecting the formation of edge states at nearly zero energy: for small systems, the edge states from opposite sides of the square dot hybridize, and the otherwise zero energy states for the semi-infinite system split in energy. As the width of the dot increases the hybridization is strongly suppressed and zero energy levels develop.

The finiteness of $\Delta(N)$ for the hexagons correlates with the finite value of U_c seen in Fig. 4. On the other hand, the

value $U_c \simeq 2.23t$ previously obtained in the literature²⁸ was determined using the fact that the density of states of bulk graphene is proportional to the absolute value of the energy relatively to the Dirac point, being zero for a half-filled system. These two results – for D_6 hexagonal clusters and the bulk system – means that the value of U_c (17) is not exclusively determined by the vanishing nature of the density of states at the Dirac point of bulk graphene. On the other hand, the two D_6 hexagons show different values of U_c , which can only be interpreted as a boundary effect, determined by the different nature of their edges. It is worth noticing that the hexagons of type HEX1, having zig-zag terminations (defining a figure with D_6 symmetry) do not develop zero energy states, leading, therefore, to the finiteness of U_c . The hexagonal dot of D_3 symmetry shows a behavior for $\Delta(N)$ identical to that found for the squares and, as a consequence, there is no finite value of U_c : the system is magnetic for any arbitrarily small value of U .

The mean-field values of U_c determined for the D_6 hexagons will be modified by quantum fluctuations. The effect of quantum fluctuations amounts in general to shifting the Hartree-Fock U_c to higher values^{28,29,31}. In the case of small graphene-based nanodots, such as bisanthrene²⁶ ($C_{28}H_{14}$), the Hubbard Coulomb interaction may be larger than that assumed for macroscopic sp^2 carbon systems. This hypothesis is based on the value $U \sim 16$ eV computed for benzene⁴⁹. Given this value and our current results, there is a real possibility of having magnetic ground states in small hexagonal systems with D_6 symmetry.

In what concerns the relation between magnetism and edge structure, we see that dots with D_3 and square symmetry have zig-zag edges, and this leads to finite magnetization for any finite U . Magnetization is maximal at, and close to, the zig-zag edges, and fades rapidly as one progresses towards the bulk of the dot. It is worth noticing that, for HEX1-type hexagonal dots, there are six external zig-zag boundaries, but its spectrum does not present zero-energy eigen values. In Fig. 3 we present particular cases of the spatial distribution of magnetization in the different dots considered in Fig. 2. For the hexagons of type HEX2 the magnetization is homogeneous over the boundary and, as soon as $U > U_c$, it develops from the boundary of the hexagon toward the bulk. For HEX1 hexagons the maximum of magnetization develops at the zig-zag vertices, but again only for $U > U_c$. In the case of the hexagon with D_3 symmetry the development of the magnetization follows the pattern of that found for HEX1 dots, but it is finite for any finite U value. The antidot case (panel (d) of Fig. 3) can be considered a simple case of a disordered system, since all symmetries are broken. In this case the magnetization develops preferentially at the internal edges connected to the bulk of the system, with formation of a *shadow* region at bottom left of the anti dot where no magnetization is seen (for that particular value of U). This behavior can be understood since the internal boundary plays, in the anti-dot, the same role as the external boundary of the equivalent dot. It is worth noticing that the anti-dot, being made of HEX1 and HEX2 hexagons has a critical Hubbard interaction, which is controlled by the U_c value of the HEX1 hexagon.

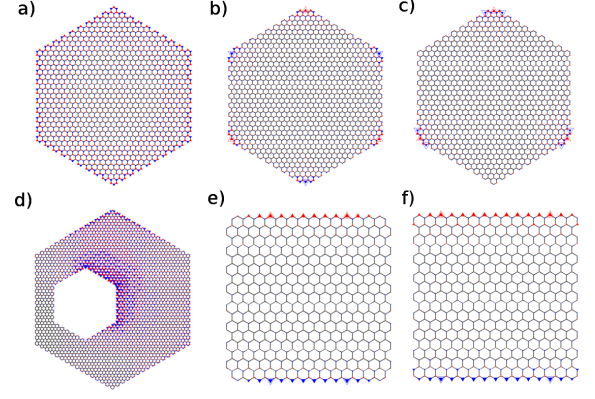


FIG. 3: (Color online) Illustration of the local magnetization for dots of the same type illustrated in Fig. 2, but with a much larger number of atoms, thus avoiding finite-size effects. Upright triangles refer to positive magnetization and the down ones to negative values. The open triangles refer to the points where the magnetization has its maximum value. In panel (a) we have a HEX2 hexagon, with $U = 2.3$; for (b) and (c) hexagons $U = 2$. In panel (d) we show an anti-dot, where the external boundary is from a HEX2 hexagon and the internal one is from a HEX1 hexagon. Panels (e) and (f) are of type SQR1 and SQR2 respectively.

In Fig. 4 we depict the dependence of the maximum of magnetization (m_{\max}) with U . We see that for the square dots of both types considered in Fig. 2 the magnetization is finite down to arbitrarily small values of U . This can be correlated with the correspondingly small values of $\Delta(N)$, shown in Fig. 5, and the behavior of the DOS at the Fermi level. As to the hexagonal dots (see Fig. 4), we also see that the existence of a finite $\Delta(N)$ is associated with the existence of a finite U_c . In other words, some geometries have finite density of states at $E = 0$, $\rho(0) \neq 0$, whereas others do not. In the case $\rho(0) = 0$ and as $N \rightarrow \infty$ the behavior of the system is essentially that of the bulk case up to finite-size corrections. On the other case, with $\rho(0) \neq 0$ for finite N , the magnetic behavior is different and there is finite magnetization for any value of U . We then understand the result obtained by Sorella and Tosatti⁽²⁸⁾ as the limiting case of $N \rightarrow \infty$ with $\rho(0) = 0$ for any finite N .

A relevant quantity to compute is the energy difference between the paramagnetic and ferromagnetic ground states, defined as

$$\Delta E = E_{\text{para}} - E_{\text{ferro}}, \quad (20)$$

where E_{para} and E_{ferro} are the ground state energies of the paramagnetic and ferromagnetic ground states. The value of ΔE is intimately related to the (mean-field) temperature at which such a magnetic ground state could be observed. In Fig. 6 the value of ΔE is given in Kelvin for both hexagons and squares. As discussed previously, these squares magnetize for any finite U and therefore we could, in principle, observe magnetism with the values of U expected for graphene (dashed lines in Fig. 6). The mean-field critical temperature is relatively high, between 10 K and 30 K, in the interval for the

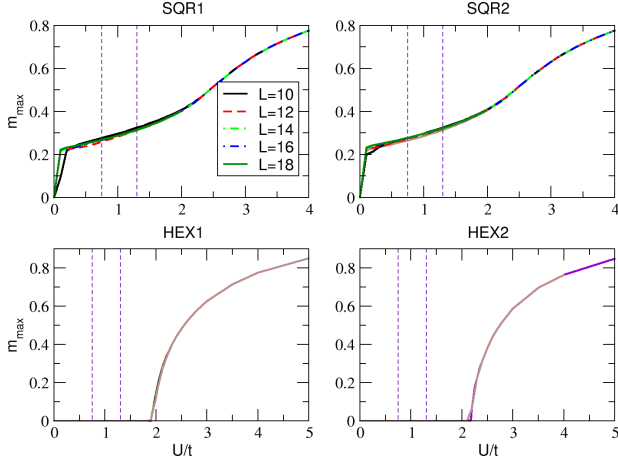


FIG. 4: (Color online) Variation of the magnetization as function of U , for squares and hexagons of different types. The vertical dashed lines refer to the values of U used in Refs. 43,51 (see text in Sec. II for a discussion about these choices).

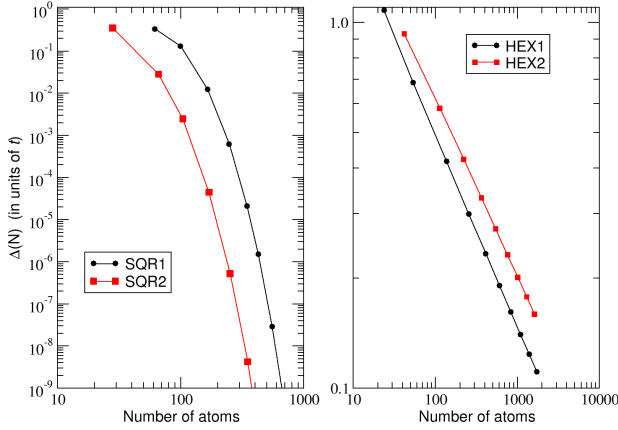


FIG. 5: (Color online) Variation of quantity $\Delta(N)$ with the number of atoms for square and hexagonal dots. From this figure alone we can understand that the spectrum of hexagons of type HEX1 and HEX2 behaves exactly in the same way, not showing the development of zero energy edge states, a consequence of the D6 symmetry alone.

lower and higher expected U in graphene, but not comparable to the room temperature magnetism observed in graphite³⁶.

IV. MAGNETISM AND STRAIN

Strain in graphene is now an active topic of experimental research. It was shown that some amount of strain can be induced either by deposition of oxide capping layers⁸ or by mechanical methods⁵⁸. The amount of strain can be determined by monitoring the blue⁸ or red⁵⁸ shifts of the G and $2D$ Raman peaks of graphene. This method is a straightforward extension of related studies used in graphite nano-fibers⁵⁹. Strain has also obvious consequences on the electronic and heat transport, producing metal-semiconductor transitions, as

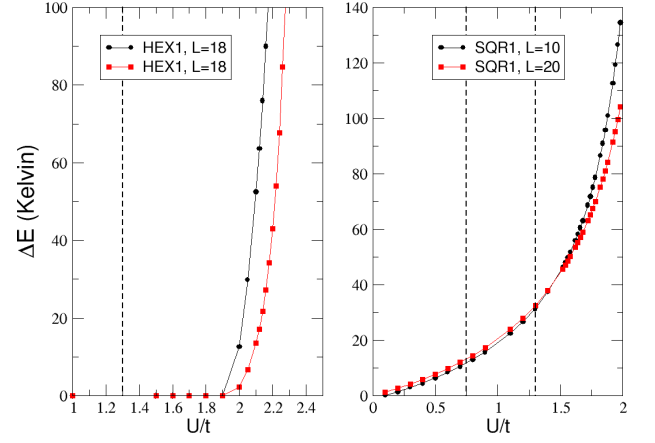


FIG. 6: (Color online) Variation of ΔE with the Coulomb interaction U/t , for hexagons of the type HEX1, and squares of the type SQR1.

in carbon nanotubes⁶⁰, or transport anisotropy in graphene⁶¹. These effects are due to changes in the band-structure of the materials as a consequence of the modification of inter-atomic distances, which in turn implies a change of the electronic hopping parameters. To our best knowledge, the first correct studies of strain effects on the bandstructure of graphene were undertaken in Ref. 47,62.

For hexagonal systems the relation between stress, σ_{ij} , and strain, u_{ij} ($i, j = x, y, z$), reads⁵⁹

$$\begin{bmatrix} u_{xx} \\ u_{yy} \\ u_{zz} \\ u_{yz} \\ u_{zx} \\ u_{xy} \end{bmatrix} = \begin{bmatrix} S_{11} & S_{12} & S_{13} & 0 & 0 & 0 \\ S_{12} & S_{11} & S_{13} & 0 & 0 & 0 \\ S_{13} & S_{13} & S_{33} & 0 & 0 & 0 \\ 0 & 0 & 0 & S_{44} & 0 & 0 \\ 0 & 0 & 0 & 0 & S_{44} & 0 \\ 0 & 0 & 0 & 0 & 0 & 2(S_{11} - S_{12}) \end{bmatrix} \begin{bmatrix} \sigma_{xx} \\ \sigma_{yy} \\ \sigma_{zz} \\ \sigma_{yz} \\ \sigma_{zx} \\ \sigma_{xy} \end{bmatrix} \quad (21)$$

where the elements $S_{i,j}$ (here $i, j = 1, 2, 3, 4$) are termed compliance constants. For the case of graphene under uniaxial tensile strain, the relation between stress and strain is

$$u_{xx} = S_{11}\sigma_{xx}, \quad (22)$$

$$u_{yy} = S_{12}\sigma_{xx}, \quad (23)$$

meaning that graphene behaves as an isotropic elastic medium. We shall consider two cases of stress: applied along the zig-zag edges (\mathcal{ZZ}), and applied along the armchair (\mathcal{AC}) edges. In these two cases, the absolute values of the next-nearest-neighbor vectors δ_i change as⁴⁷

$$|\delta_{1,3}| = 1 + \frac{3}{4}\varepsilon - \frac{1}{4}\varepsilon\nu, \quad (24)$$

$$|\delta_2| = 1 - \varepsilon\nu, \quad (25)$$

for the \mathcal{ZZ} case, and

$$|\delta_{1,3}| = 1 + \frac{1}{4}\varepsilon - \frac{3}{4}\varepsilon\nu, \quad (26)$$

$$|\delta_2| = 1 + \varepsilon, \quad (27)$$

for the \mathcal{AC} case, where $\varepsilon = S_{11}\sigma$ is the amount of longitudinal strain, and $\nu = -S_{12}/S_{11}$ is the Poisson ratio. The two

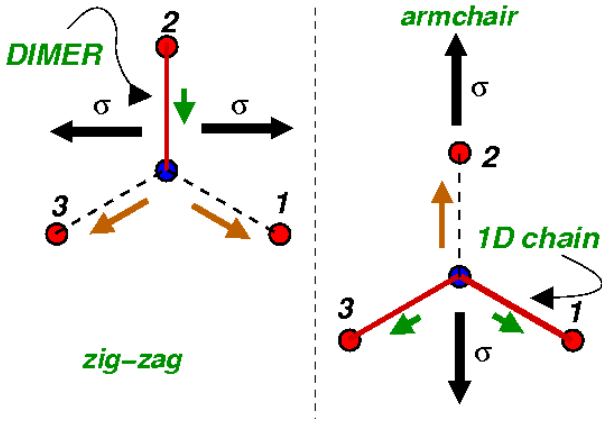


FIG. 7: (Color online) Representation of the effect of stress on the length of the nearest neighbors carbon atoms. On the left we depict the \mathcal{ZZ} case, and, on the right, the \mathcal{AC} one. For the \mathcal{ZZ} case, the stress σ induces an increase of the hopping associated with the vertical bond, due to the Poisson effect. The hoppings associated with bonds 1 and 3 are reduced, and the system tends to dimerize at large deformations. For tension along \mathcal{AC} , σ is oriented along bond 2. In this case all hoppings are reduced, but the one associated with bond 2 decreases more than the other two, leading to a set of quasi one-dimensional chains. The quantitative change of the hoppings upon stress was studied quantitatively using *ab-initio* methods in Ref. [62].

cases correspond to two different physical situations, which can be understood in the case of extreme deformations using a simple picture: in the \mathcal{ZZ} case the system tends to dimerize, since $|\delta_{1,3}|$ lengthen, and $|\delta_2|$ shortens; in the \mathcal{AC} case, all three distances lengthen, but $|\delta_2|$ lengthens more, which can be construed as a tendency for the formation of quasi one-dimensional structures. A real space picture representing these two situations can be seen in Fig. 7.

In Fig. 8 we present results regarding the effect of strain on the magnetization of the dots. For the purpose of illustration we consider dots of smaller size, but the results of Fig. 4 guarantee that we should have negligible finite-size effects. The global effect of tensile stress on the edge magnetization of the dot is an increase of its magnitude, independently of whether we consider stress along \mathcal{ZZ} or \mathcal{AC} directions. In quantitative terms, the magnetization increase is more pronounced when stress is applied in the \mathcal{ZZ} configuration than on the \mathcal{AC} one. In experimental terms, the prediction is that magnetism in graphene-based systems should be easier to detect when the material is under stress.

Figure 9 shows the explicit variation of U_c with strain, for the hexagons of type HEX, which have a finite U_c . In the same figure, on the bottom row, the effect of ε on the maximum of the magnetization, m_{\max} , is also represented for squares of the type SQR2 (which have no critical U). We observe an increase of m_{\max} as ε increases. The dependence of m_{\max} on ε is not the same for the \mathcal{ZZ} and \mathcal{AC} cases at the same U value. Stress along the zig-zag edge is most effective at producing an enhancement of m_{\max} . This behavior can be understood on the basis of the qualitative physical picture described in Fig. 7: stress along zig-zag edges tends to pro-

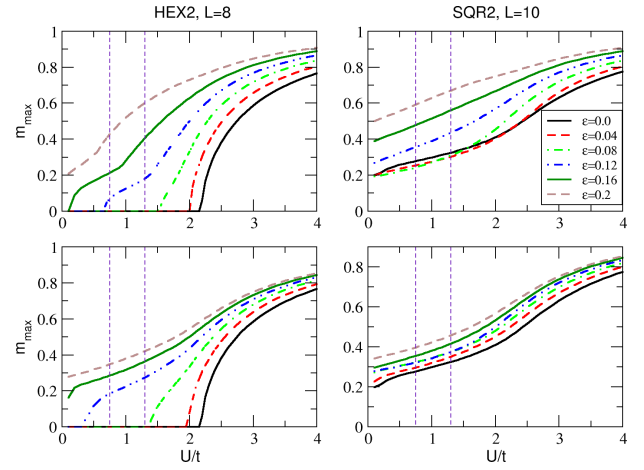


FIG. 8: (Color online) Variation of the magnetization as function of the Hubbard interaction U , for different strain values ε . The top panels refer to stress along the \mathcal{ZZ} edge and the other to stress along the \mathcal{AC} edge. The Poisson ratio used was that of a PET substrate ($\nu \simeq 0.3$), considered in study of the Raman red shift of the G and $2D$ peaks of graphene⁵⁸. The vertical dashed lines refer to the values of U used in Refs. 43,51 (see text in Sec. II for a discussion about these choices).

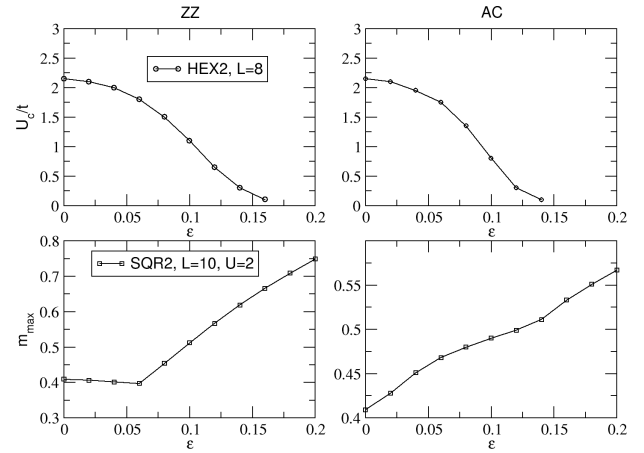


FIG. 9: (Color online) Variation of the critical value, U_c , with the amount of strain, for the cases \mathcal{ZZ} (top left) and \mathcal{AC} (top right). In both cases we used HEX2-type hexagons with $L = 8$. In the bottom row we have the dependence of the maximum value of magnetization, m_{\max} , on the amount of strain, using $U/t = 2$, and for the cases \mathcal{ZZ} (down left) and \mathcal{AC} (down right). In both cases we used SQR2-type squares, with $L = 10$.

duce dimmers weakly coupled between them, which favors the magnetic state at those tightly bound atoms.

For hexagons with a finite U_c , Fig. 8 shows that the overall effect of strain along both the \mathcal{ZZ} and \mathcal{AC} cases is to reduce the value of U_c , which for large ε obeys $U_c \ll t$. At first sight this result may seem easy to understand: the value of U cannot change with stress because it is a local (on-site) property⁶³. The hopping, on the other hand, depends strongly on the inter-atomic distance, and hence on the external stress. Since the result for U_c in the bulk system, Eq. (17), is bound to

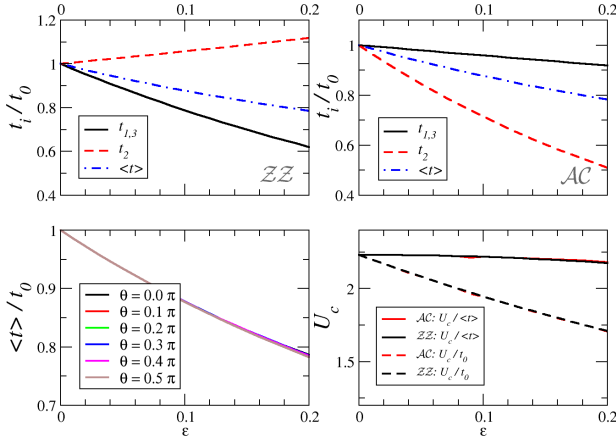


FIG. 10: (Color online) The top row shows the variation of the nearest neighbor hoppings $t_{1,2,3}$ and the average hopping, $\langle t \rangle$ under uniaxial strain, with strain applied along the ZZ (left) and AC directions (right). The bottom left panel consists of the variation of $\langle t \rangle$ with strain, for different orientations of the uniaxial deformation. In the last panel on the bottom right we present U_c/t_0 and $U_c/\langle t \rangle$ for the two representative directions.

the value of the (uniform) hopping t , a change in t produces a change in the absolute value of U_c . If we had an uniform magnetic ground state (as would be the case for bulk graphene without zig-zag edges), the effect of external stress could be captured through the average hopping $\langle t \rangle$, which diminishes as ϵ increases, causing a reduction of the critical value of the Hubbard interaction, $U_c(\epsilon) \sim \alpha \langle t(\epsilon) \rangle$ [α should be around 2.23, as per eq. (17)]. Since we measure energies in units of the bare t , the above can be written as

$$\frac{U_c(\epsilon)}{t} \sim \alpha \frac{\langle t(\epsilon) \rangle}{t}, \quad (28)$$

and thus $U_c(\epsilon)/t$ would be expected to follow the variation of $\langle t \rangle$ with strain.

To verify to which extent such effects contribute to the results shown in Fig. 8 we have calculated the critical Hubbard interaction expected for a uniform graphene system, as a function of magnitude and direction of strain. Within the Hartree-Fock framework U_c is given by²⁸

$$\frac{1}{U_c} = \frac{1}{N} \sum_{\mathbf{k}} \frac{1}{|E(\mathbf{k})|} \quad (29)$$

where N is the total number of carbon atoms, and $E(\mathbf{k})$ the non-interacting electron dispersion. In the presence of strain we will have a generalized dispersion given by

$$E(\mathbf{k}) = \pm |t_2 + t_3 e^{-i\mathbf{k} \cdot \mathbf{a}_1} + t_1 e^{-i\mathbf{k} \cdot \mathbf{a}_2}|, \quad (30)$$

reflecting that the nearest neighbor hoppings, t_i , can all be different in general⁴⁷. Using the parameterization introduced in reference 47, we have extracted U_c as a function of strain magnitude, ϵ , and orientation with respect to the honeycomb lattice, θ ($\theta = 0$ for ZZ , and $\theta = \pi/2$ for AC).

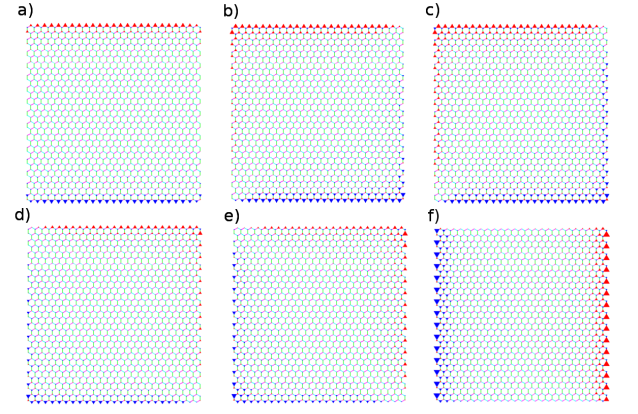


FIG. 11: (Color online) Spatial variation of the magnetization as function of strain. (a) $\epsilon = 0$; (b) and (c) corresponds to $\epsilon = 0.14, 0.22$, with stress along the armchair edge; (d), (e), (f) corresponds to $\epsilon = 0.10, 0.14, 0.22$, with stress along the zig-zag edge. In both cases there is an increase of the magnetization along the armchair edge as ϵ increases. The upright triangles represent positive magnetization and the down ones represent negative values.

Figures 10(a,b) show how the three hopping integrals t_1 , t_2 and t_3 vary under uniaxial strain along the ZZ and AC directions, respectively. Also included in those panels, are the respective average values of the hopping, defined as the arithmetic mean of the three nearest neighbor hopping integrals. It can be seen that the average hopping, $\langle t \rangle$, is essentially the same for both ZZ and AC . This is shown more clearly in Fig. 10(c), where we plot $\langle t \rangle$ as a function of strain, and for different strain directions: there is no sensible modification of $\langle t \rangle$ as the angle θ defining the tension direction is changed. Notwithstanding, the tendency is for $\langle t \rangle$ to decrease, as we naturally expect. The critical values of U_c under strain are shown in Fig. 10(d), where we plot both U_c/t_0 (that reflects the absolute variation in the critical coupling), and $U_c/\langle t \rangle$ (which reflects the statement in eq. (28)). On the one hand, the fact that $U_c/\langle t \rangle$ is roughly constant up to deformations of 20% tallies with the assumption in eq. (28) using a constant parameter α . However, even though the decrease in U_c/t_0 with strain shown in Fig. 10(d) is qualitatively in agreement with the discussion above regarding the behavior of U_c for the dots in Fig. 9, the curves in Fig. 10(d) do not decrease as rapidly. Hence, the above argument that the critical U should follow the variation of $\langle t \rangle$ (28), is not quantitatively accurate.

The reason for this lies in the very nature of the magnetic ground states of the quantum dots, which are not uniform. Consequently, the above argument fails in quantitative accuracy, because it assumes uniformity. Similarly to what happens in nanoribbons, the magnetization in the dots studied here has a strong space dependence, being highly enhanced near certain edges. This is a direct consequence of the character of the electron states around the Fermi energy, which tend to be localized near the boundaries. Moreover, as the dots are deformed by the applied strain, this space distribution is affected as well. In Fig. 11 we show the spatial evolution of the magnetization at the edges of the dots of type SQR2 as

ε increases. We have chosen representative values of ε such that the effect is clearly evident. Stress along either the armchair edge (panels (b) and (c) in Fig. 11), or the zig-zag edge (panels (d), (e) and (f) in Fig. 11) shows the same trend: a tendency for magnetization transfer from the zig-zag to the armchair edge of the dot. The effect is more pronounced for tension along the \mathcal{ZZ} as shown in Figs. 11(d-f). In all cases, the value of the magnetization increases, as can be seen in the lower panels of Fig. 9. From the picture described in Fig. 7, the behavior of the magnetization in the \mathcal{ZZ} case can be understood as follows: large stress along zig-zag edges tends to produce quasi-dimers, weakly connected to each other; the dimers at the armchair edges are only coupled to the bulk of the dot by two weak bonds, and this favors the stabilization of a magnetic state.

V. DISCUSSION

In this paper we have studied magnetism in graphene quantum dots of particular geometries, with and without zig-zag edges. Similarly to what has been proposed in the context of graphene nanoribbons, the magnetism displayed by these systems may be used in spin filters. We have not studied the effect of leads on the ferromagnetic order, but the broadening of the quantum dot levels due to coupling to the leads (a system with a continuous spectrum), will have an impact on the magnetic properties of the dot. In the case of a ferromagnetic nanoparticle, a theoretical description has already been developed⁶⁴, but no such model exists for graphene to our best knowledge. This study will be the subject of a forthcoming publication. Another aspect we have not considered in our study is the effect of the substrate on the magnetic properties of the dot. Since graphene dots are meant to be used as nanoelectronic devices, they will always interact with some substrate, which can reduce thermal fluctuations, and favor magnetism at finite temperatures.

It is worth stressing again the main reason for magnetism at the edges of some graphene systems. Thinking about graphene ribbons or dots as a bulk system, that is by looking at the total density of states, leads immediately to the objection that magnetism should not be present for any finite U value. However, by looking at our results for magnetism in these systems it is clear that this is a property of the edges. Therefore the relevant quantity is not the bulk density of states, but rather the local density of states, and this latter quantity, near the edges, does become very large at the Fermi energy ($E = 0$), thus leading to very small critical U values (eventually indistinguishable from zero). This shows that the total density of states is not a relevant quantity for this problem.

Ab-initio calculations have shown that very small benzene-based systems, such as bisanthrene, have ferromagnetic ground states, and therefore we expect that magnetism will also be present in small quantum dots of graphene, as hinted by our Hartree-Fock results. We have also seen how stress might affect the magnetic ground states. When applied along the zig-zag edges, stress seems to promote a spatial rearrangement the magnetization distribution throughout the dot. This,

combined with the transport response of these systems, may allow mechanical control over spin-polarized currents flowing inside the dot. On the other hand, the fact that stress along zig-zag edges leads to the formation of dimers weakly coupled between them, suggests that the system may prefer to form a sort of spin liquid. Investigations of whether the ground state will be truly magnetic or a spin liquid are required.

In our calculations including strain, we have resorted to linear elasticity to describe the lattice deformations, as reported in reference 47. We now wish to justify its validity, since it is an important point and deserves a careful explanation. We do not expect linear theory to remain valid for deformations as high as the 20% used in some of our calculations above. However, since we are interested solely in the influence of strain in the electronic structure, and not on the detailed elastic response, the relevant detail is not the validity of the linear theory itself, but rather how a certain amount of strain changes the hopping values. In our calculations we combined linear theory with the widespread parameterization of the dependence of the $V_{pp\pi}$ on the carbon-carbon distance

$$V_{pp\pi}(l) = te^{-3.37(l-1)}, \quad (31)$$

where l is the length of the stretched (or compressed) carbon-carbon distance, in units of that undeformed distance. From the above equation what matters really is the quantity $(l - 1)$, which is determined by the amount of strain, and its prefactor in the argument of the exponential. Since there might be legitimate doubts with respect to the use of linear elasticity for determining l in the above equation, this issue was addressed in another publication⁶². There, first principles calculations were used to study the effect of strain on the nearest-neighbor hopping values. By their nature, first principles calculations make no use of any elastic approximation, being valid for arbitrary deformations, in principle. It was found that the combined use of linear theory and of the above formula for $V_{pp\pi}$ gives accurate results for the hopping values. Moreover, as discussed in reference 47 subsequent *ab-initio* calculations have shown good quantitative agreement with the use of linear elasticity combined with the parameterization (31) (for example the merging of the two Dirac points for tension along the zigzag direction is predicted to occur at the same values of strain, around 25%, both *ab-initio* and within tight-binding with linear elasticity). Therefore our approach to the calculation of the hopping variation upon strain, and its consequences for the π -bandstructure is accurately captured by the linear theory.

The impact of edge roughness on the magnetic properties of the dots also deserves some considerations. In graphene nanostructures prepared with current fabrication techniques, the edges are invariably rough and disordered. This can hinder the stability of long range magnetic order. However much is still unknown with respect to the nature of edge reconstruction in real graphene nanostructures. It is expected that the chemical bonds at the edges be under (surface) tension, which leads to edge reconstruction as a means of relieving elastic energy. This reconstruction could lead to self-organization of the edge, reducing the roughness and allowing for long range magnetic order. Moreover, the recent advances in tai-

loring, at the atomic level, sub-nanostructures by transmission electron microscope⁵⁷, might allow unprecedented control over the edge profiles. Having such control will certainly add greater tangibility to the prospect of tailoring magnetic states in graphene nanostructures.

Finally, we point out that the experimental observation of ferromagnetism arising from grain boundaries with zig-zag edges in graphite strongly suggests that dimensionality is not a paramount issue in carbon-based systems, as long as some mechanism for quenching the thermal and quantum fluctuations is present. Besides the anisotropy in the interaction between the local magnetic moments³⁶, the fact that graphene is generally deposited onto a substrate could provide an extra quenching mechanism, in the same way that

it suppresses the fluctuation-induced crumpling of the two-dimensional graphene membrane. The mechanical stability of graphene and the robustness of its magnetic phases can be seen as a vivid example of fluctuation quenching.

Acknowledgments

We thank Antonio H. Castro Neto for stimulating discussions. N.M.R.P. was supported by FCT under Grant No. PTDC/FIS/64404/2006. V.M.P was partially supported by the U.S. DOE under the grant DE-FG02-08ER46512.

- ¹ R. F. Service, *Science* **324**, 875 (2009).
- ² N. M. R. Peres, *Eur. Phys. News*, **40**, Nr 3, 17 (2009).
- ³ K. S. Novoselov, A. K. Geim, S. V. Morozov, D. Jiang, Y. Zhang, S. V. Dubonos, I. V. Grigorieva, and A. A. Firsov, *Science* **306**, 666 (2004).
- ⁴ K. S. Novoselov, D. Jiang, T. Booth, V.V. Khotkevich, S. M. Morozov and A. K. Geim, *PNAS* **102**, 10451 (2005).
- ⁵ A. H. Castro Neto, F. Guinea, N. M. R. Peres, K. S. Novoselov, and A. K. Geim, *Rev. Mod. Phys.* **81**, 109 (2009).
- ⁶ A. A. Balandin, S. Ghosh, W. Bao, I. Calizo, D. Teweldebrhan, F. Miao, C. N. Lau, *Nano Lett.* **8**, 902 (2008).
- ⁷ Tim J. Booth, Peter Blake, Rahul R. Nair, Da Jiang, Ernie W. Hill, Ursel Bangert, Andrew Bleloch, Mhairi Gass, Kostya S. Novoselov, M. I. Katsnelson, and A. K. Geim, *Nano Lett.* **8**, 2442 (2008).
- ⁸ Zhen Hua Ni, Hao Min Wang, Yun Ma, Johnson Kasim, Yi Hong Wu, and Ze Xiang Shen, *ACS Nano* **2**, 1033 (2008).
- ⁹ Changgu Lee, Xiaoding Wei, Jeffrey W. Kysar, and James Hone *Science* **321**, 385 (2008).
- ¹⁰ Keun Soo Kim, Yue Zhao, Houk Jang, Sang Yoon Lee, Jong Min Kim, Kwang S. Kim, Jong-Hyun Ahn, Philip Kim, Jae-Young Choi, and Byung Hee Hong, *Nature* **457**, 706 (2009).
- ¹¹ R. M. Westervelt, *Science* **320**, 324 (2008).
- ¹² J. Scott Bunch, Yuval Yaish, Markus Brink, Kirill Bolotin, and Paul L. McEuen, *Nano Lett.* **5**, 287 (2005).
- ¹³ F. Miao, S. Wijeratne, Y. Zhang, U. C. Coskun, W. Bao, and C. N. Lau, *Science* **317**, 1530 (2007).
- ¹⁴ C. Stampfer, J. Göttinger, F. Molitor, D. Graf, T. Ihn, and K. Ensslin, *Appl. Phys. Lett.* **92**, 012102 (2008).
- ¹⁵ L. A. Ponomarenko, F. Schedin, M. I. Katsnelson, R. Yang, E. W. Hill, K. S. Novoselov, and A. K. Geim, *Science* **320**, 356 (2008).
- ¹⁶ J. Tworzydło, B. Trauzettel, M. Titov, A. Rycerz, and C.W.J. Beenakker *Phys. Rev. Lett.* **96**, 246802 (2006).
- ¹⁷ F. Muñoz-Rojas, D. Jacob, J. Fernández-Rossier, and J. J. Palacios, *Phys. Rev. B* **74**, 195417 (2006).
- ¹⁸ Masayuki Yamamoto, Yositake Takane, and Katsunori Wakabayashi, *Phys. Rev. B* **79**, 125421 (2009).
- ¹⁹ M. I. Katsnelson, and F. Guinea, *Phys. Rev. B* **78**, 075417 (2008).
- ²⁰ Z. Z. Zhang, Kai Chang, and F. M. Peeters, *Phys. Rev. B* **77**, 235411 (2008).
- ²¹ Jürgen Wurm, Adam Rycerz, Inanç Adagideli, Michael Wimmer, Klaus Richter, and Harold U. Baranger, *Phys. Rev. Lett.* **102**, 056806 (2009).
- ²² J. Akola, H. P. Heiskanen, and M. Manninen *Phys. Rev. B* **77**, 193410 (2008).
- ²³ Katsunori Wakabayashi, *Phys. Rev. B* **64**, 125428 (2001).
- ²⁴ Melinda Y. Han, Barbaros Özyilmaz, Yuanbo Zhang, and Philip Kim *Phys. Rev. Lett.* **98**, 206805 (2007).
- ²⁵ Young-Woo Son, Marvin L. Cohen, and Steven G. Louie, *Phys. Rev. Lett.* **97**, 216803 (2006).
- ²⁶ Oded Hod, Verónica Barone, and Gustavo E. Scuseria, *Phys. Rev. B* **77**, 035411 (2008).
- ²⁷ Eduardo V. Castro, N. M. R. Peres, and J. M. B. Lopes dos Santos, *J. Optoelectron. Adv. Materials* **10**, 1716 (2008).
- ²⁸ S. Sorella and E. Tosatti, *Europhys. Lett.* Vol **19**, 699 (1992).
- ²⁹ L. M. Martelo, M. Dzierzawa, L. Siffert, and D. Baeriswyl, *Z. Physik B* **103**, 335 (1997).
- ³⁰ N. M. R. Peres, M. A. N. Araújo, and Daniel Bozi, *Phys. Rev. B* **70**, 195122 (2004).
- ³¹ Thereza Paiva, R. T. Scalettar, W. Zheng, R. R. Singh, and J. Oitmaa, *Phys. Rev. B* **72**, 085123 (2005).
- ³² Eduardo V. Castro, N. M. R. Peres, T. Stauber, and N. A. P. Silva, *Phys. Rev. Lett.* **100**, 186803 (2008).
- ³³ T. Stauber, Eduardo V. Castro, N. A. P. Silva, and N. M. R. Peres, *J. Phys.: Cond. Matt.* **20**, 335207 (2008).
- ³⁴ J. Barzola-Ququia, P. Esquinazi, M. Rothermel, D. Spemann, T. Butz, and N. Garcia, *Phys. Rev. B* **76**, 161403 (2007).
- ³⁵ H. Ohldag, T. Tylliszczak, R. Höhne, D. Spemann, P. Esquinazi, M. Ungureanu, and T. Butz, *Phys. Rev. Lett.* **98**, 187204 (2007).
- ³⁶ J. Červenka, M. I. Katsnelson, and C. F. J. Flipse, *Nat. Phys.* (AOP, doi:10.1038/nphys1399).
- ³⁷ V. Yu. Irkhin, A. A. Katanin, and M. I. Katsnelson, *Phys. Rev. B* **60**, 1082 (1999).
- ³⁸ Mitsutaka Fujita, Katsunori Wakabayashi, Kyoko Nakada, and Koichi Kusakabe, *J. Phys. Soc. Jpn.* **65**, 1920 (1996) (and references therein).
- ³⁹ J. Fernández-Rossier and J. J. Palacios, *Phys. Rev. Lett.* **99**, 177204 (2007).
- ⁴⁰ F. Muñoz-Rojas, J. Fernández-Rossier, and J. J. Palacios *Phys. Rev. Lett.* **102**, 136810 (2009).
- ⁴¹ J. J. Palacios, J. Fernández-Rossier, and L. Brey *Phys. Rev. B* **77**, 195428 (2008).
- ⁴² Grigory Tkachov, *Phys. Rev. B* **79**, 045429 (2009).
- ⁴³ Oleg V. Yazyev, *Phys. Rev. Lett.* **101**, 037203 (2008).
- ⁴⁴ N. M. Peres, F. Guinea, and A. H. Castro Neto, *Phys. Rev. B* **73**, 125411 (2006).
- ⁴⁵ Vitor M. Pereira, F. Guinea, J. M. B. Lopes dos Santos, N. M. R. Peres, and A. H. Castro Neto, *Phys. Rev. Lett.* **96**, 036801 (2006).

- ⁴⁶ Vitor M. Pereira and A. H. Castro Neto, Phys. Rev. Lett. **103**, 046801 (2009).
- ⁴⁷ Vitor M. Pereira, A. H. Castro Neto, and N. M. R. Peres, Phys. Rev. B **80**, 045401 (2009).
- ⁴⁸ H. Q. Lin and J. E. Hirsch, Phys. Rev. B **35**, 3359 (1987).
- ⁴⁹ R. G. Parr, D. P. Craig, and I. G. Ross, J. Chem. Phys. **18**, 1561 (1950).
- ⁵⁰ Dionys Baeriswyl, David K. Campbell, and Sumit Mazumdar, Phys. Rev. Lett. **56**, 1509 (1986).
- ⁵¹ J. Jung and A. H. MacDonald, Phys. Rev. **79**, 235433 (2009).
- ⁵² Rainer Strack and Dieter Vollhardt, Phys. Rev. Lett. **72**, 3425 (1994).
- ⁵³ A. P. Kampf and A. A. Katanin, Phys. Rev. B **67**, 125104 (2003).
- ⁵⁴ M. A. Vozmediano, M. P. López-Sancho, T. Stauber, and F. Guinea, Phys. Rev. B **72**, 155121 (2005).
- ⁵⁵ P. W. Brouwer, E. Racine, A. Furusaki, Y. Hatsugai, Y. Morita, and C. Mudry Phys. Rev. B **66**, 014204 (2002).
- ⁵⁶ Vitor M. Pereira, J. M. B. Lopes dos Santos, and A. H. Castro Neto Phys. Rev. B **77**, 115109 (2008)
- ⁵⁷ Chuanhong Jin, Haiping Lan, Lianmao Peng, Kazu Suenaga, and Sumio Iijima, Phys. Rev. Lett **102**, 205501 (2009).
- ⁵⁸ T. M. G. Mohiuddin, A. Lombardo, R. R. Nair, A. Bonetti, G. Savini, R. Jalil, N. Bonini, D.M. Basko, C. Galiotis, N. Marzari, K. S. Novoselov, A. K. Geim, and A. C. Ferrari, Phys. Rev. B, **79**, 205433 (2009).
- ⁵⁹ H. Sakata, G. Dresselhaus, and M. S. Dresselhaus, J. Appl. Phys. **63**, 2769 (1988).
- ⁶⁰ E. D. Minot, Yuval Yaish, Vera Sazonova, Ji-Yong Park, Markus Brink and Paul L. McEuen, Phys. Rev. Lett. **90**, 156401 (2003).
- ⁶¹ K. S. Kim, Y. Zhao, H. Jang, S. Y. Lee, J. M. Kim, K. S. Kim, J.-H. Ahn, P. Kim, J.-Y. Choi, and B. H. Hong, Nature (London) **457**, 706 (2009).
- ⁶² R. M. Ribeiro, Vitor M. Pereira, N. M. R. Peres, P. R. Briddon, and A. H. Castro Neto, New J. Phys. (in press).
- ⁶³ We have discussed in Sec. II how the Hubbard U should be understood as an effective interaction term. In this sense, strain can in principle modify the non-local contributions. However, the local terms are always dominant, and so, as a first approximation, we can say that deformations of the lattice do not affect sensibly the value of U .
- ⁶⁴ Denis M. Basko and Maxim G. Vavilov, Phys. Rev. B **79**, 064418 (2009).